Cerebral Cortex Advance Access published January 22, 2016

OXFORD

Cerebral Cortex, 2016, 1–13

doi: 10.1093/cercor/bhv310
Original Article

ORIGINAL ARTICLE

cAMP-Dependent Calcium Oscillations of Astrocytes: An Implication for Pathology

Sakiko Ujita[1], Takuya Sasaki[1], Akiko Asada[1], Kenta Funayama[1], Mengxuan Gao[1], Katsuhiko Mikoshiba[2], Norio Matsuki[1] and Yuji Ikegaya[1,3]

[1]Graduate School of Pharmaceutical Sciences, The University of Tokyo, Tokyo, Japan, [2]Laboratory for Developmental Neurobiology, Riken Brain Science Institute, Saitama, Japan and [3]Center for Information and Neural Networks, Suita City, Osaka, Japan

*Address correspondence to Yuji Ikegaya, Laboratory of Chemical Pharmacology, Graduate School of Pharmaceutical Sciences, The University of Tokyo, 7-3-1 Hongo, Bunkyo-ku, Tokyo 113-0033, Japan. Email: ikegaya@mol.f.u-tokyo.ac.jp

Downloaded from http://cercor.oxfordjournals.org/ at University of Tokyo Library on January 22, 2016

Abstract

Astrocytes in various brain regions exhibit spontaneous intracellular calcium elevations both in vitro and in vivo; however, neither the temporal pattern underlying this activity nor its function has been fully evaluated. Here, we utilized a long-term optical imaging technique to analyze the calcium activity of more than 4000 astrocytes in acute hippocampal slices as well as in the neocortex and hippocampus of head-restrained mice. Although astrocytic calcium activity was largely sparse and irregular, we observed a subset of cells in which the fluctuating calcium oscillations repeated at a regular interval of ~30 s. These intermittent oscillations i) depended on type 2 inositol 1,4,5-trisphosphate receptors; ii) consisted of a complex reverberatory interaction between the soma and processes of individual astrocytes; iii) did not synchronize with those of other astrocytes; iv) did not require neuronal firing; v) were modulated through cAMP-protein kinase A signaling; vi) were facilitated under pathological conditions, such as energy deprivation and epileptiform hyperexcitation; and vii) were associated with enhanced hypertrophy in astrocytic processes, an early hallmark of reactive gliosis, which is observed in ischemia and epilepsy. Therefore, calcium oscillations appear to be associated with a pathological state in astrocytes.

Key words: astrocyte, cAMP, calcium oscillation

Introduction

Astrocytes spontaneously exhibit various forms of intracellular calcium elevations. This activity has been observed both in vitro and in vivo and appears across different spatiotemporal scales (Volterra et al. 2014). Increased calcium levels have been implicated in the release of gliotransmitters as well as in the modulation of cerebral blood flow (Mulligan and MacVicar 2004; Gordon et al. 2008; Girouard et al. 2010) and neuronal activity (Jourdain et al. 2007; Henneberger et al. 2010; Navarrete and Araque 2010; Takata et al. 2011; Min and Nevian 2012). In pathological states, the release of gliotransmitters induces excitotoxicity and cell death (Ding et al. 2007; Agulhon et al. 2012; Lee et al. 2013; Kawamata et al. 2014).

Although extensive studies have been conducted regarding the functional role and mechanism of astrocytic calcium activity, these studies have focused mainly on calcium activity that is artificially evoked through electrical stimulation, agonist perfusion, or photo-uncaging (Fiacco et al. 2009; Hamilton and Attwell 2010; Volterra et al. 2014). These "evoked" calcium transients might be insufficient to reproduce the physiological features of calcium signaling in astrocytes. Nevertheless, the description of spontaneous calcium activity remains limited to its spatial characteristics (Aguado et al. 2002; Hirase et al. 2004; Kuga et al. 2011; Sasaki, Kuga et al. 2011), and its temporal characteristics, heterogeneity, and the nature of interactions between astrocytes remain largely unknown. Compared with neuronal electrical activity, astrocytic calcium activity is far slower; its time-scale

© The Author 2016. Published by Oxford University Press. All rights reserved. For Permissions, please e-mail: journals.permissions@oup.com

ranges from tens of seconds to minutes. Thus, the temporal dynamics of astrocytic activity might be overlooked in conventional small-scale, short-duration recordings.

In general, intracellular calcium signaling is made more complicated by its interaction with other second messengers, such as cyclic adenosine monophosphate (cAMP). The involvement of cAMP signaling in astrocytic morphology (Segovia et al. 1994; Vardjan et al. 2014) is well known, and more recently, the involvement of Gs protein-coupled signaling in astrocytic modulation of learning and memory has received considerable attention (Orr et al. 2015). However, surprisingly, crosstalk between calcium and cAMP signaling remains to be evaluated in astrocytes.

In the present study, we evaluated the temporal characteristics of spontaneous astrocytic calcium activity using a large-scale, long-term optical imaging technique. From sequences of spontaneous calcium activity that were captured for as long as 90 min from hundreds of cells, we report a unique temporal pattern of astrocytic calcium activity, that is, cell-autonomous, intermittent calcium oscillations (IOs). Interestingly, IO activity was sparse under the default-mode condition but was facilitated through the stimulation of cAMP signaling and under pathological conditions.

Materials and Methods

The experiments were performed with the approval of the animal experimental ethics committee at the University of Tokyo (approval number: P24-8) and in accordance with the guidelines for the care and use of laboratory animals.

Hippocampal Slice Preparations

Postnatal 9- to 12-day-old ICR mice (SLC) or type 2 inositol 1,4,5-trisphosphate receptor knockout (IP_3R2-KO) mice were anesthetized with ether and decapitated. The brains were immersed in ice-cold modified artificial cerebrospinal fluid (aCSF) composed of 27 mM $NaHCO_3$, 1.4 mM NaH_2PO_4, 2.5 mM KCl, 7.0 mM $MgSO_4$, 1.0 mM $CaCl_2$, 222 mM sucrose, and 0.5 mM ascorbic acid, which was bubbled with 95% O_2 and 5% CO_2. Horizontal entorhinal-hippocampal slices were carefully cut at a thickness of 400 µm using a vibratome. All slices were cut at 80 µm/s. The slices were maintained at 37°C for 20 min in normal aCSF composed of 127 mM NaCl, 26 mM $NaHCO_3$, 1.6 mM KCl, 1.24 mM KH_2PO_4, 1.3 mM $MgSO_4$, 2.4 mM $CaCl_2$, and 10 mM glucose.

Calcium Imaging from Astrocytes

Oregon Green 488 BAPTA-1 (OGB1) AM was used to monitor cytosolic calcium dynamics. Note that unlike other calcium indicators, such as fluo4 and fura-red, OGB1 AM is not preferentially taken up by intracellular organelles (Thomas et al. 2000). The slices were incubated at room temperature for 40 min with 5 µg/mL OGB1 AM (Invitrogen), 100 µg/mL Pluronic F-127 (Invitrogen), and 50 µg/mL Cremophor EL (Sigma–Aldrich) and were then incubated in aCSF for >60 min. Subsequently, the slices were placed in a recording chamber for >10 min, and spontaneous calcium signals were recorded from astrocytes in the CA1 stratum radiatum and stratum lacunosum-moleculare. The chamber was perfused with aCSF at 3–4 mL/s. The fluorophores were excited at 488 nm, and images were recorded at 1 Hz using a cooled EM-CCD camera (iXonEM + DV897; Andor Technology) using a water-immersion objective lens (×16 or ×40, 0.8 NA, Nikon) and a Nipkow-disk confocal laser scanner (CSU-10/X1; Yokogawa Electric). Slices that moved >3 µm in the z-axis were discarded, whereas slices that moved in the *x*–*y* dimension were corrected post hoc using ImageJ software (National Institutes of Health) and custom-written MATLAB scripts (MathWorks). The fluorescence intensity within OGB1-labeled cells was almost homogenous throughout the entire cell and did not exhibit subcellular localization due to dye accumulation in intracellular organelles. Furthermore, only activity that occurred throughout the entire somatic structure was analyzed to avoid contamination of calcium elevations in organelles; therefore, any calcium elevations that were confined to a part of the soma or processes were discarded. Based on the immunoreactivity of glial fibrillary acidic protein (GFAP), regions of interest (ROIs) were carefully and manually set to avoid selecting nonastrocytic structures. The mean fluorescence intensity was measured from the soma of each astrocyte, and changes were defined as $\Delta F/F_0 = (F_t - F_0)/F_0$, where F_t is the fluorescence intensity at time t and F_0 is the baseline, which was averaged for 50 s before and after time t. Calcium increases were semiautomatically extracted with a threshold of 4% $\Delta F/F_0$ (Sasaki et al. 2008; Sasaki, Kuga et al. 2011). The 4% level corresponded to the 2 × SD of the noise fluctuations; the SD was estimated from the below-peak distribution of the noise based on the assumption that the noise conformed to a Gaussian distribution. All calcium events were carefully inspected by eye to ensure that the events corresponded to somatic calcium elevations in astrocytes. Because OGB1 AM usually labels astrocytes as well as neurons, astrocyte signals that were extracted using the above procedure could be contaminated with neuronal calcium activity; however, astrocytic and neuronal calcium transients can be discriminated based on their temporal profiles. Compared with neurons, astrocytes usually exhibit calcium signals with slower kinetics (Ikegaya et al. 2005); astrocytic calcium levels usually rise and drop on the order of seconds to tens of seconds, whereas neuronal calcium levels increase more sharply (typically within 100 ms) and drop within a second. In addition, the amplitudes of glial calcium transients are much larger than those of neuronal calcium transients. Therefore, the calcium events analyzed here almost exclusively reflected the activity of astrocytes.

Immunohistochemistry and Analysis of Astrocytic Morphology

The slices were fixed in either 4% paraformaldehyde in 0.1 m phosphate buffer for 2 h or in 40 mg/mL 1-ethyl-3-(3-dimethylaminopropyl)carbodiimide hydrochloride (EDC) in 0.1 m phosphate buffer solution for 3–6 h at room temperature. EDC preserves OGB1 inside the cell throughout immunohistochemistry procedures (Tymianski et al. 1997). Slices that were fixed with paraformaldehyde were washed with PBS, whereas the EDC-fixed slices were washed with 0.1 m glycine in PBS. After the slices were blocked with 5–10% goat serum and 0.1–0.3% Triton X-100 for 60 min, they were incubated with a primary rabbit monoclonal antibody against GFAP (1:500; Dako or Sigma–Aldrich) or a primary mouse monoclonal antibody against S100β (1:1000; Sigma–Aldrich) overnight at 4°C and then labeled with a secondary antirabbit IgG Alexa Fluor 594 (1:400; Invitrogen). The sections were imaged using a confocal microscope (FV 1200; Olympus) with a water-immersion objective lens (×20 or ×40; Olympus) and an Ar/Kr or He-Ne laser. Super-resolution images were obtained using FV-OSR technology (Olympus), an oil-immersion objective lens (×100; Olympus), and a laser diode.

Application of Drugs

Tetrodotoxin (Wako), suramin (Sigma–Aldrich), MCPG (Sigma–Aldrich), KT5720 (Sigma–Aldrich), forskolin (Sigma–Aldrich),

Downloaded from http://cercor.oxfordjournals.org/ at University of Tokyo Library on January 22, 2016

propranolol (Wako), and isoproterenol (Wako) were bath-applied at concentrations of 1, 100, 500, 0.03, 50, 50, and 10 μm, respectively. For treatment with tetrodotoxin, suramin, MCPG, propranolol, and KT5720, the drugs were perfused from −5 min and throughout the recordings. Bath application was performed under fluid velocities of 3–4 mL/s. For treatment with 30 μm cyclopiazonic acid (Wako) and o-nitrophenyl-EGTA (NP-EGTA; Invitrogen), the slices were incubated in aCSF containing the drug for 10–15 min. (1S,3R)-1-aminocyclopentane-1,3-dicarboxylic acid (ACPD; Tocris) was locally applied using a glass pipette.

Application of Electrical Stimulation

For electrical stimulation, a glass pipette filled with aCSF was carefully placed in the stratum radiatum of CA1, and high-frequency stimulation (HFS; 100 pulses at 100 Hz, 100 μA) was applied. The activity in cells within 100 μm of the pipette was analyzed.

Acute Pathological Models

Ischemia-like neuronal network states were induced through oxygen-glucose deprivation (OGD), under which aCSF was continuously bubbled with 95% N_2 and 5% CO_2 and glucose was replaced with sucrose. Epileptic-like hyperexcitation states were induced with Mg^{2+}-free aCSF containing 50 μm picrotoxin (Sigma–Aldrich).

In Vivo Calcium Imaging in Astrocytes

For anesthetized in vivo recordings, male ICR mice aged postnatal 20–30 days were anesthetized with urethane (1.5 g/kg, i.p.) and implanted with a metal head-holding plate. The depth of anesthesia was evaluated based on the lack of paw withdrawal, whisker movement, and eye blink reflex. A small craniotomy (1×1 mm^2), which was centered at 2.0 mm posterior and 2.0 mm lateral to bregma, was made, and the dura was surgically removed. Then, the exposed cortical surface was loaded with a small volume (up to 500 μL) of dye solution containing 0.125% fluo4-AM (Invitrogen), 100 μm SR101 (Invitrogen), 20% DMSO, and 8% Pluronic F-127. During an incubation period of 45–60 min, the cortical surface was covered with a small piece of gel foam. Subsequently, the unloaded dye was washed with aCSF, and the surface was covered with 2% agar dissolved in aCSF. For awake recordings, the mice were anesthetized with ketamine (50 mg/kg, i.p.) and xylazine (10 mg/kg, i.p.). After a metal head-holding plate was implanted, the mice were subjected to head-fixation training for 5–10 days as previously described (Ishikawa et al. 2014; Funayama et al. 2015). The mice were again anesthetized with a ketamine/xylazine cocktail, and craniotomy and dye loading were subsequently performed. After the mice recovered from anesthesia, recordings were made under head fixation. Astrocytic calcium activity was recorded at 1 frame/s using a two-photon microscope with a water-immersion objective lens (16×, 0.8 NA or 25×, 1.05 NA) (Kuga et al. 2011). Throughout the experiment, a heating pad maintained the rectal temperature at 37°C.

Carotid Artery Occlusion

Cerebral ischemia was induced by unilateral occlusion of the carotid artery. A mouse was anesthetized with urethane, and the carotid artery ipsilateral to the two-photon-imaged hemisphere was exposed. During imaging, the artery was occluded using polyester thread #50 (Daiso). The occlusion was initiated 5 min after the onset of the calcium imaging and remained in place for the rest of the imaging period.

Data Analysis

All statistical procedures were performed using MATLAB software. Cell morphology was analyzed using ImageJ. The data are presented as the means ± SEMs unless otherwise specified. Paired *t*-tests, Student's *t*-tests, Dunnett's tests, Kolmogorov–Smirnov tests, and one-way repeated-measures ANOVA were performed to assess significance. $P < 0.05$ was considered statistically significant.

Results

Characterization of Astrocytic Calcium Oscillations

We conducted functional imaging of calcium activity from 97 ± 4 astrocytes in acute hippocampal slices that were loaded with OGB1 AM (mean ± SEM of 43 slices from 32 mice). We utilized a Nipkow-disk confocal microscope, which rapidly scans a wide microscopic field at low laser intensity. The laser intensity on the slice surface was set between 4 and 19 μW, and a setting of 10 μW was typically used to avoid phototoxicity or photobleaching (Kuga et al. 2011); notably, the mean laser intensity used in a Nipkow-disk microscope is substantially lower than that used in two-photon or conventional confocal microscopes; thus, this type of microscope is suitable for long-lasting imaging. The cells were classified post hoc based on GFAP immunoreactivity (Fig. 1A). On average, 20.2 ± 1.3% of the imaged astrocytes were spontaneously active in any 20-min period of control recordings ($n = 33$ control slices). The percentage of active cells and the overall frequency of activity were constant throughout the duration of the recordings, which lasted for as long as 90 min, ruling out ongoing damage to the slices caused by the imaging procedure.

In a subset of astrocytes, we discovered a characteristic pattern of oscillatory bursts, that is, oscillatory cycles of calcium transients (Fig. 1B, *magenta dots*). Figure 1C shows a return map, or a scatter plot of consecutive interactivity intervals (IAIs) in the space of the *n*th IAI versus the $(n + 1)$th IAI, for a representative oscillatory cell, demonstrating that the oscillation events (*magenta circles*) formed a cluster and were distinct from other sporadic events (gray circles). We pooled all datasets from 33 slices and plotted these measurements in a single return map using a pseudocolored scale (Fig. 1D). The IAI distribution exhibited a peak at <60 s. Thus, we defined an IO event as a group of >2 calcium transients that repeated at an interactivity interval of <60 s (Fig. 1E).

On average, 4.5 ± 0.3% of the total astrocytes, which corresponded to 34 ± 3.8% of the active astrocytes, exhibited IOs (mean ± SEM of 33 slices). In single cells, IO events occurred at a mean frequency of 0.17 ± 0.03 per hour (mean ± SEM of 3507 cells); in active cells, the events occurred at a frequency of 0.80 ± 0.13 per hour (mean ± SEM of 711 cells). Among the 2328 total calcium transients in 33 control slices, 1012 events (43%) were classified as IOs, whereas the remaining 57% of events occurred sporadically. A single oscillation event lasted for 86.0 ± 7.0 s and consisted of 4.9 ± 0.3 calcium transients (mean ± SEM of 208 events). Compared with sporadic activity, transients involved in IOs were significantly larger in terms of $\Delta F/F_0$ amplitude (IO: 6.7 ± 0.2%, $n = 1012$ transients, sporadic: 6.3 ± 0.1%, $n = 1316$ transients; $P = 0.042$, $t_{2326} = 2.03$, Student's *t*-test) and shorter in duration (IO: 16.1 ± 0.39 s, sporadic: 28.2 ± 0.8 s; $P = 6.2 \times 10^{-35}$, $t_{2326} = 12.5$, Student's *t*-test).

Downloaded from http://cercor.oxfordjournals.org/ at University of Tokyo Library on January 22, 2016

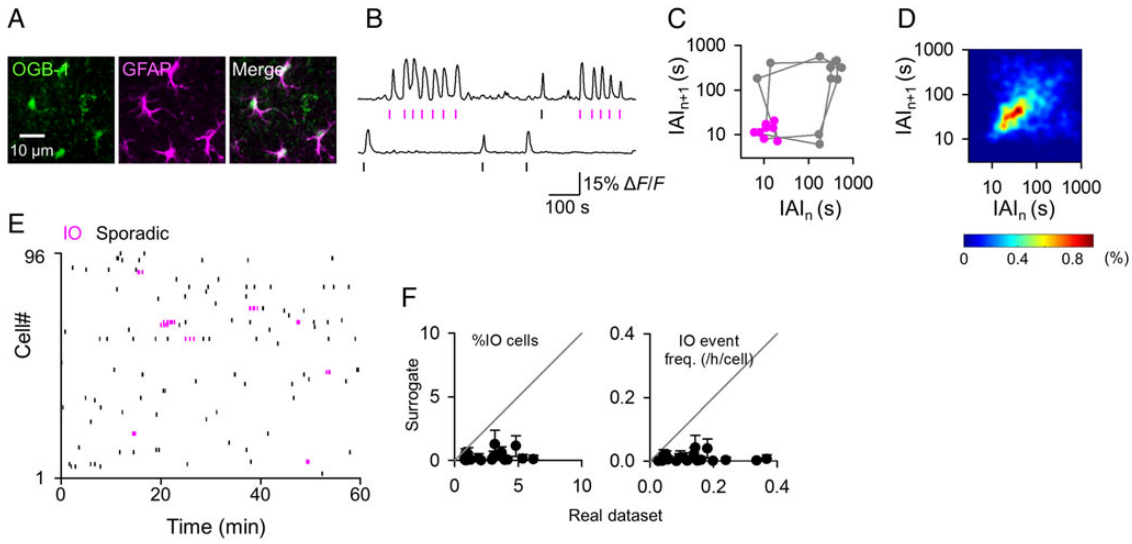

Figure 1. Spontaneous calcium oscillations in hippocampal CA1 astrocytes. (*A*) OGB1-loaded cells were immunolabeled post hoc with an anti-GFAP antibody. (*B*) Two representative $\Delta F/F_0$ traces showing IOs (*top*) and sporadic events (*bottom*). The vertical bars below the traces indicate the onset times of individual calcium transients; the *magenta bars* correspond to IOs. (*C*) Representative return map of interactivity intervals (IAIs) in a single astrocyte that was recorded for 60 min. The $(n + 1)$th IAI was plotted against the nth IAI. The *magenta circles* indicate IAIs during IOs. (*D*) The 2-dimensional distribution of the first IAIs and the mean of the subsequent IAIs are shown using a pseudocolored scale. (*E*) Representative raster plot of 96 astrocytes that were simultaneously monitored for 60 min. Each dot indicates a single calcium transient. The *magenta dots* indicate IOs. (*F*) The proportion of IO cells (*left*) to the total number of monitored cells and the mean frequency of IO events per cell (*right*) were higher than those observed in the surrogates. Each data point indicates a single dataset ($n = 22$ slices). The error bars represent the SDs of 1000 surrogates.

To examine whether the IOs occurred by chance, we generated 1000 surrogate datasets after shuffling the calcium events in each original dataset. More specifically, one calcium transient in a given cell was exchanged with one randomly selected event from another randomly selected cell without changing the timing of the events; this activity swapping between 2 cells was repeated for the entire dataset. This procedure preserved both the frequency of activity in individual cells and the population modulation of event timings (Ikegaya et al. 2004; Sasaki et al. 2007). In all datasets, the activity-swapped surrogates contained significantly fewer IO cells and IO events than the actual datasets (Fig. 1*F*). Thus, the occurrence of IOs cannot be explained by chance. Furthermore, IOs were also observed in in vivo preparations from the primary visual cortex of awake (Supplementary Fig. 1*A*; % cells: 23.2 ± 11.8; event frequency: 0.92 ± 0.34 events/h/cell) and anesthetized (Supplementary Fig. 1*B*; % cells: 14.13 ± 5.07; event frequency: 0.38 ± 0.16 events/h/cell) young adult mice and from the hippocampus of anesthetized young adult mice (Supplementary Fig. 1*C*; % cells: 7.86 ± 2.24; event frequency: 0.42 ± 0.14 events/h/cell). Thus, IOs were not limited to slices prepared from juvenile mice; rather, they are likely to occur regardless of preparation, brain region, or animal age.

Cellular Mechanisms of IOs

We assessed the basic characteristics of IOs using pharmacological and genetic approaches. Consistent with previous reports (Parri et al. 2001; Nett et al. 2002), we confirmed that bath application of 1 μm tetrodotoxin did not alter either the frequency of overall activity (Fig. 2*A*; $P = 0.32$, $t_4 = 0.26$, paired *t*-test; $n = 5$ slices) or the frequency of sporadic activity (Fig. 2*B*; $P = 0.89$, $t_4 = 0.15$). In addition, tetrodotoxin did not affect either the percentage of IO cells (Fig. 2*C*; $P = 0.98$, $t_4 = 0.02$) or the frequency of IO events (Fig. 2*D*; $P = 0.75$, $t_4 = 0.34$). Thus, the spontaneous astrocytic IOs occurred independently of neuronal spiking activity. Furthermore, tetanic stimulation of Schaffer collaterals in the striatum radiatum did not reliably induce IOs in nearby cells (Supplementary Fig. 2*A*,*B*), which is consistent with the idea that neuronal firing itself does not directly trigger IOs.

We next examined whether the occurrence of IO events was based on extracellular neurotransmitters, such as ATP and glutamate. Bath application of 100 μm suramin, a nonspecific purinergic receptor antagonist, did not affect the occurrence of overall calcium activity (Fig. 2*A*; $P = 0.77$, $t_4 = 0.30$, $n = 5$ slices), sporadic activity (Fig. 2*B*; $P = 0.76$, $t_4 = 0.31$), or IOs (Fig. 2*C*,*D*; % cells: $P = 0.67$, $t_4 = 0.44$; event frequency: $P = 0.64$, $t_4 = 0.49$). In contrast, the application of 500 μm MCPG, a group I and II metabotropic glutamate receptor antagonist significantly reduced the frequency of both sporadic (Fig. 2*B*; $P = 0.049$, $t_4 = 2.31$, $n = 5$ slices) and IO activity (Fig. 2*C*,*D*; % cells: $P = 0.032$, $t_4 = 2.57$; event frequency: $P = 0.007$, $t_4 = 3.62$). These results suggest that extracellular glutamate is the basis of general calcium elevation in astrocytes, whereas ATP is not involved in the generation of calcium activity, including IOs. According to this observation, local application of 100 μM ACPD, a group I and II metabotropic glutamate receptor agonist, induced transient oscillations in 72 ± 21% of astrocytes (Supplementary Fig. 2*H*, mean ± SEM of 10 slices).

We also investigated the calcium source of IOs. IOs were completely abolished after treatment with 20 μm cyclopiazonic acid, a specific inhibitor of Ca^{2+}-ATPase in the endoplasmic reticulum (Fig. 2*C*,*D*; $n = 5$ slices). Moreover, IOs did not occur in slices that were prepared from mice lacking the IP_3R2 channel (IP_3R2-KO mice), which mediates intracellular calcium release in astrocytic somata (Sharp et al. 1999; Holtzclaw et al. 2002) (Fig. 2*C*,*D*; $n = 5$ slices). These data suggest that the IOs depended on IP_3R2-mediated calcium release. Interestingly, a small number of sporadic oscillations persisted in both cyclopiazonic acid-treated slices and IP_3R2-KO slices (Fig. 2*A*,*B*). Direct stimulation of astrocytes using NP-EGTA, a UV-sensitive caged-calcium reagent (Sasaki, Matsuki et al. 2011), triggered IO-like phenomena, which were completely abolished in slices that were prepared from IP_3R2-KO mice (Supplementary Fig. 2*C*,*E*,*F*).

Downloaded from http://cercor.oxfordjournals.org/ at University of Tokyo Library on January 22, 2016

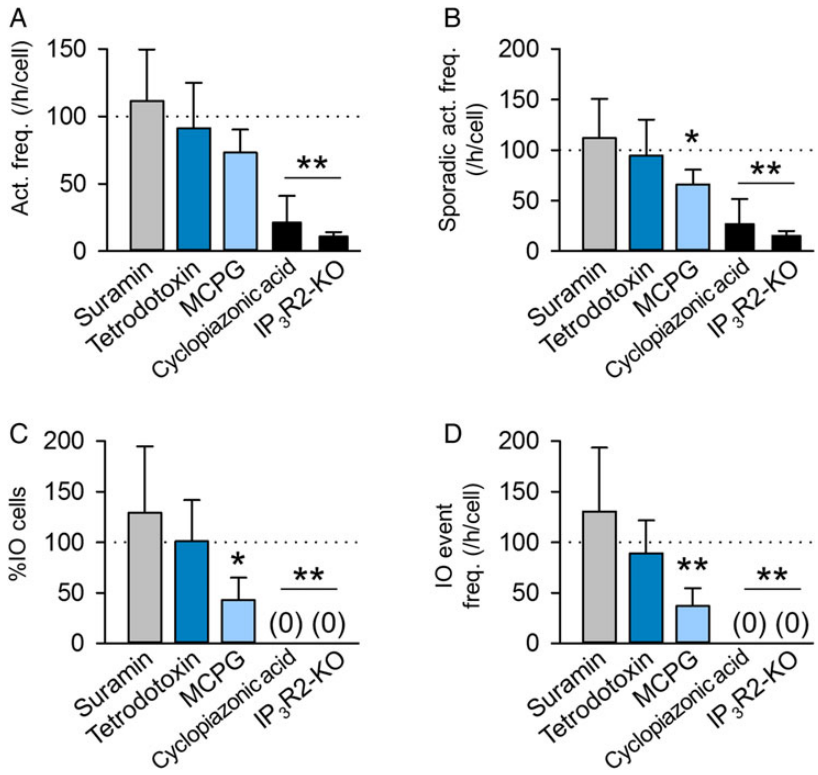

Figure 2. Profiles of astrocytic calcium oscillations. (*A–D*) Frequency of all transients per cell (*A*), frequency of sporadic events (*B*), percentage of IO cells (*C*), and frequency of IO events (*D*) relative to control in 100 μM suramin-treated, 1 μm tetrodotoxin-treated, 500 μM MCPG-treated, and 20 μM cyclopiazonic acid-treated slices and in slices prepared from IP_3R2-KO mice. The values were normalized to the control. $^{**}P < 0.01$ and $^{*}P < 0.05$ versus control, paired *t*-test or Student's *t*-test. The error bars indicate the SEM of 5 slices per condition.

Astrocytes form a syncytium by interacting with adjacent cells via gap junctions and gliotransmitters (Giaume et al. 2010; Giaume and Liu 2012). To examine whether IOs emerged through astrocytic network interactions, we focused on the spatio-temporal correlations between these events. Figure 3A presents a representative cell map in which IO cells are shown in *magenta*. To examine whether the IO cells were spatially clustered, we compared the distances between IO cells in actual datasets and those in 1000 surrogate datasets in which the same number of astrocytes were randomly selected from the original cell map. The distance distribution did not differ between the original datasets and the surrogates (Fig. 3*B*, *left*). Considering that synchrony and the propagation of calcium events typically occur in neighboring cells (Kuga et al. 2011; Sasaki, Kuga et al. 2011), we compared the distances between pairs of cells that simultaneously exhibited oscillations and observed no differences between the real datasets and the 1000 surrogates (Fig. 3*B*, *right*). Thus, IOs were not clustered in space or synchronized between neighboring cells.

To examine whether IOs occurred due to network-level modulations of excitation, we computed the coefficient of variation (CV) of the number of cells that showed IO events at each moment (Fig. 3*C*, bin = 1 s). The CVs did not differ between the original datasets and the activity-swapped surrogates (Fig. 3*D*). Furthermore, the probability of the occurrence of an IO relative to the IO event of a given cell was calculated to assess the temporal correlations (Fig. 3*E*, *left*, bin = 1 min). IOs were evenly distributed before and after a given IO event, indicating that IOs occurred independently of each other. This held true for IO-to-sporadic and sporadic-to-sporadic analyses (Fig. 3*E* *middle* and *right*, respectively), indicating that both IOs and sporadic activity reflected single-cell-level behavior, independent of other astrocytes.

Notably, the application of TTX did not alter either the spatial distribution of IO cells (Supplementary Fig. 3A) or the temporal profile of IOs (Supplementary Fig. 3B), further supporting the independence of this phenomenon from neuronal firing.

Intracellular Dynamics of IOs

Considering that the IOs occurred at the single-cell level, we next focused on intracellular calcium dynamics during IOs. We first detected IO cells using large-scale imaging and subsequently observed the somata and processes using a higher-magnification objective. The morphology of these subcellular structures was confirmed post hoc through electroporation with Alexa Fluor 594 (Fig. 4A) (Reeves et al. 2011). Figure 4*B* shows representative line-scan plots of calcium transients along 3 primary processes of an astrocyte. During single IO events, 78 ± 25% of processes exhibited calcium oscillations together with somatic oscillatory events (Fig. 4C; mean ± SEM of 11 cells). This ratio was higher than that found for processes involved in sporadic activity (Fig. 4C, $P = 0.03$, $t_{34} = 1.96$, Student's *t*-test). In addition, IO events were more frequently initiated from a sporadic event in astrocyte processes (Fig. 4*D*). Therefore, during a typical IO event, the initial activity of one astrocytic process propagated to the soma and subsequently propagated to more processes, resulting in a ping-pong-like reverberation between the soma and the processes. Thus, the direction of activity propagation was not necessarily uniform across individual cycles of an IO event; IOs consisted of a complex mixture of soma-to-process and

Downloaded from http://cercor.oxfordjournals.org/ at University of Tokyo Library on January 22, 2016

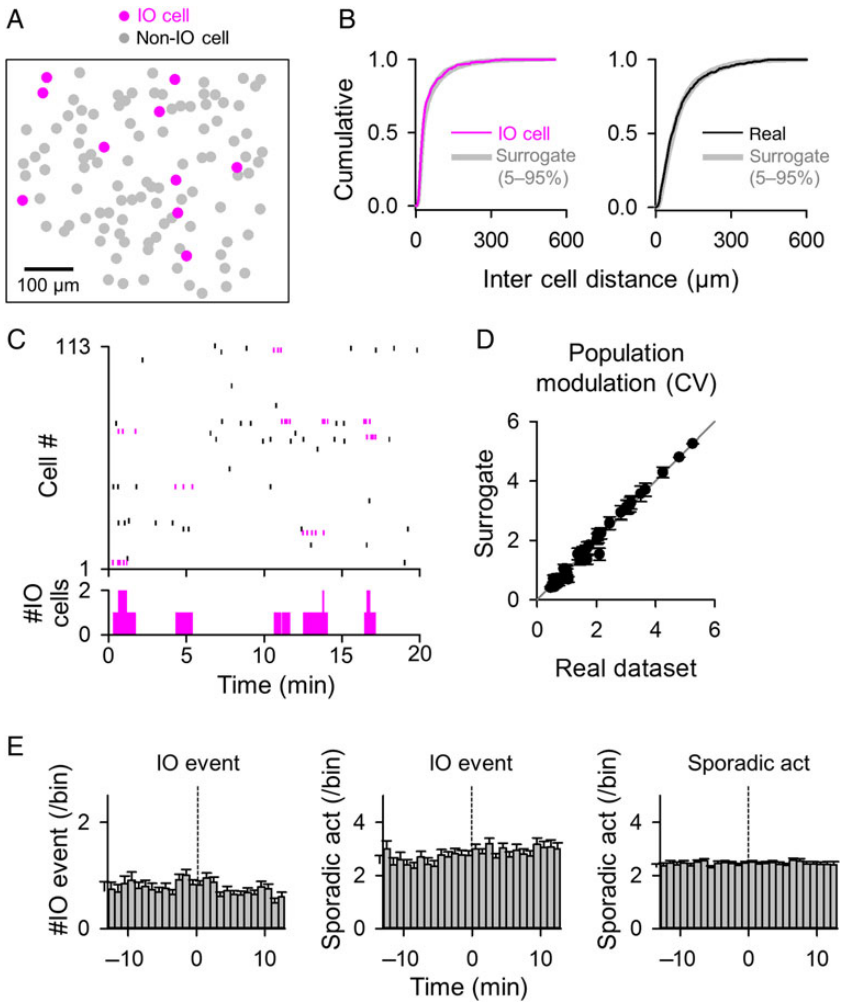

Figure 3. Lack of correlation across intercellular IOs. (*A*) Representative map of astrocytes in the CA1 stratum radiatum. IO cells are shown in *magenta*. (*B*) *Left*, cumulative probability distribution of the distance from an IO cell to the nearest other IO cell. The data are pooled from 640 IO cell pairs from 35 slices. *Right*, cumulative distribution of the intercell distance between pairs of synchronously oscillating cells. The data are pooled from 921 IO cell pairs from 25 slices. The *gray* shadow indicates the 5–95% confidence interval that was obtained from 1000 surrogates. (*C*) IO events, which are indicated in *magenta* in the *top* raster plot, are collapsed to the *bottom* histogram of the number of IO cells for a given 1-s time period. (*D*) The CV of the number of cells that showed IO events at a given time period is compared with that computed for the surrogates. Each data point indicates a single dataset. The error bars indicate the SD of 1000 surrogates. (*E*) Triggered average plot of IOs and sporadic activity. The occurrence of an IO event relative to a given IO event (*left*), of a sporadic event to an IO event (*middle*), and of a sporadic event to a sporadic event (*right*) were calculated. The error bars indicate the SDs of 208 IO cells and 1249 non-IO cells.

process-to-soma propagations. In a small number of rare cases, we observed local oscillations that occurred only in processes and did not propagate to the soma (Fig. 4*E*).

Molecular Mechanisms of IOs

A variety of cell types exhibit oscillatory calcium elevations that depend on IP_3 signaling (Li et al. 1995; Mikoshiba 2011). Like astrocytes, hepatocytes and parotid acinar cells express IP_3R2 and exhibit calcium oscillations (Woods et al. 1986; Wojcikiewicz et al. 1994; Bruce et al. 2002). These oscillations are associated with cAMP and protein kinase A (PKA) (Chatton et al. 1998; Bruce et al. 2002; Soltoff and Hedden 2010). Therefore, we examined the involvement of the cAMP-PKA pathway in astrocytic calcium oscillations using KT5720, a PKA inhibitor (Fig. 5A). Neither the frequency of the total calcium transients (Fig. 5B; $P = 0.20$, $t_5 = 1.48$, paired *t*-test) nor the frequency of sporadic events (Fig. 5C; $P = 0.61$, $t_5 = 0.55$) was significantly altered after bath application of 30 nm KT5720 ($n = 6$ slices). In contrast, KT5720 significantly reduced both the percentage of cells that exhibited IOs (Fig. 5D, $P = 0.0027$, $t_5 = 5.49$) and the frequency of IO events (Fig. 5E, $P = 0.024$, $t_5 = 3.20$). The effect of KT5720 was only partial, consistent with the low concentration applied; notably, the IC_{50} of KT5720 for PKA was shown to be 60 nm (Kase et al. 1987). Nonetheless, the effectiveness of KT5720 at the low concentration of 30 nm suggests that PKA activity underlies the generation of IOs; notably, at higher concentrations, KT5720 might act as a nonspecific inhibitor of kinases.

To examine whether the activation of cAMP signaling was sufficient to induce IOs in astrocytes, we bath-applied 50 μm forskolin, an activator of adenylate cyclase, for 5 min (Fig. 6A). Forskolin increased the overall calcium activity in astrocytes (Fig. 6B; $P = 7.1 \times 10^{-4}$, $t_4 = 9.40$ paired *t*-test; $n = 5$ slices) and induced IOs in 47 ± 4% astrocytes (Fig. 6B; mean ± SEM of 5 slices; % cells: $P = 0.25 \times 10^{-3}$, $t_4 = 6.74$; event frequency: $P = 0.0011$, $t_4 = 8.45$, paired *t*-test). After the drug was washed out, the increased calcium activity gradually returned to baseline levels within 80 min (Fig. 6A, *bottom*). The overall ratios of the 3 types

Downloaded from http://cercor.oxfordjournals.org/ at University of Tokyo Library on January 22, 2016

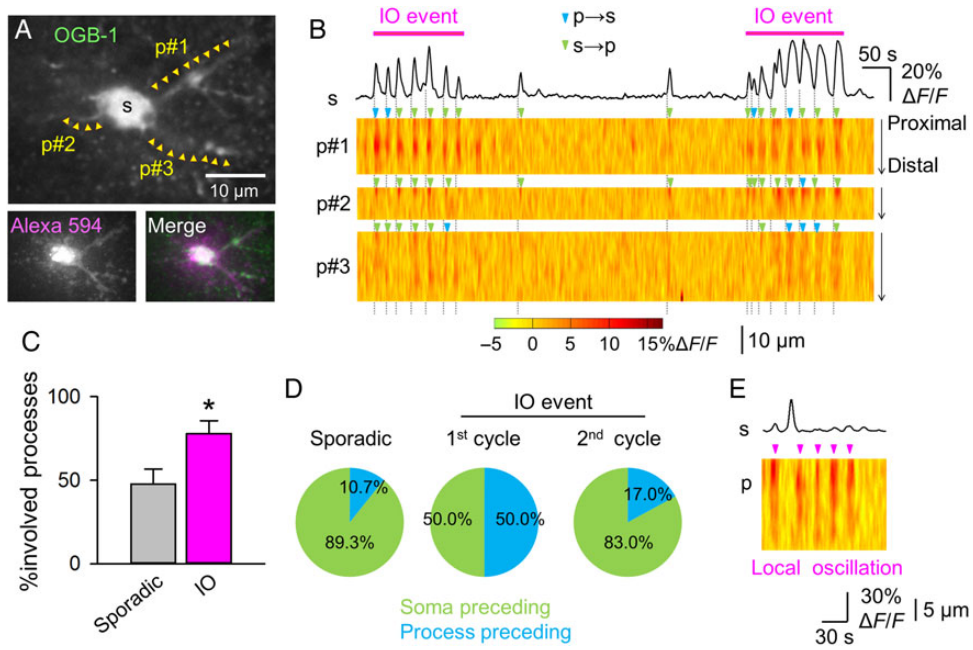

Figure 4. Intracellular calcium waves during IOs. (*A*) Confocal images of an astrocyte, the morphology of which was identified via electroporation with Alexa Fluor 594. (*B*) Fluorescence changes in the soma (*top trace*) and in the 3 processes shown in *A* (*bottom XT-scans*). The dotted lines in the background indicate the onset times of the somatic calcium transients. The *green* arrowheads indicate calcium transients that propagated from the soma (*s*) to the processes (*p*), whereas the *blue* arrowheads indicate transients that propagated from a process to the soma. (*C*) The percentage of processes that exhibited sporadic and IO calcium transients relative to the total number of imaged processes. $^{*}P = 0.03$, $t_{34} = 1.96$, Student's *t*-test. The error bars show the SEM of 28 sporadic events and 8 IO events in 11 astrocytes in 5 slices. (*D*) The ratios of soma- and process-initiated sporadic and IO calcium events. $n = 28$ sporadic events, 8 transients in the first oscillation cycle, and 47 transients in the second and subsequent cycles. (*E*) Local calcium oscillations that occurred in the processes (*p*) and not in the soma (*s*).

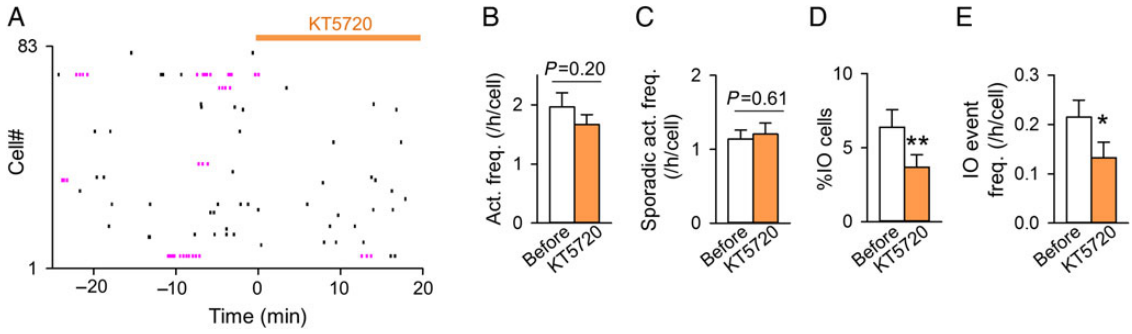

Figure 5. PKA dependence of astrocytic calcium IOs. (*A*) Representative raster plot of spontaneous calcium transients. KT5720 was continuously bath-applied after time 0 min. The *magenta dots* indicate IOs. (*B–E*) Frequency of total transients per cell (*B*), frequency of sporadic events (*C*), percentage of IO cells (*D*), and frequency of IO events (*E*) before and after KT5720 treatment. $^{*}P = 0.024$, $t_5 = 3.20$, $^{**}P = 0.0027$, $t_5 = 5.49$ vs. before, paired *t*-test. Error bars indicate the SEM of 6 slices.

of astrocytic calcium dynamics, that is, IO activity, sporadic activity, or no activity, remained constant in the untreated control slices (Supplementary Fig. 4A, *top*). These ratios were identical before and after the application of forskolin, although the ratios of IO cells increased during forskolin application (Supplementary Fig. 4A, *bottom*). Thus, although forskolin-induced hysteretic state perturbations, the astrocytes' net state remained stable. The states of individual astrocytes spontaneously shifted under control conditions (Supplementary Fig. 4B, *top*), and such shifts were also observed in the forskolin-treated group (Supplementary Fig. 4B, *bottom*). However, the transition rates did not significantly differ between the control and forskolin-treated groups ($P > 0.1$, *Z*-test for multiple proportions).

Astrocytes express β-adrenergic receptors (Salm and McCarthy 1992), the activation of which can increase cAMP in astrocytes via the G protein α subunit Gs. Indeed, we observed that a 5-min application of 10 μm isoproterenol, a β-adrenergic receptor agonist, replicated the effect of forskolin and induced IOs in 44 ± 6% astrocytes (Fig. 6*B*; mean ± SEM of 5 slices; % cell: $P = 0.97 \times 10^{-4}$, $t_4 = 8.68$; event frequency: $P = 0.0012$, $t_4 = 8.29$, paired *t*-test). Thus, both direct and endogenous receptor-mediated stimulation of the cAMP-dependent pathway induced IOs. KT5720 (30 nm) significantly reduced the frequency of IO events (Fig. 6*C*; $P = 0.035$, $t_{13} = 2.66$, Dunnett's test after one-way ANOVA; $n = 6$ slices), although this inhibitor did not affect the percentage of cells that exhibited IOs in response to forskolin (Fig. 6*C*; $P = 0.96$, $t_{13} = 0.24$). Notably, KT5720 shortened the duration of the persistence of IOs after forskolin washout (Fig. 6*D*). In slices prepared from IP_3R2-KO mice, forskolin did not induce IOs (Fig. 6*C*; $n = 5$ slices). Incidentally, the basal level of IOs was not perturbed by

Downloaded from http://cercor.oxfordjournals.org/ at University of Tokyo Library on January 22, 2016

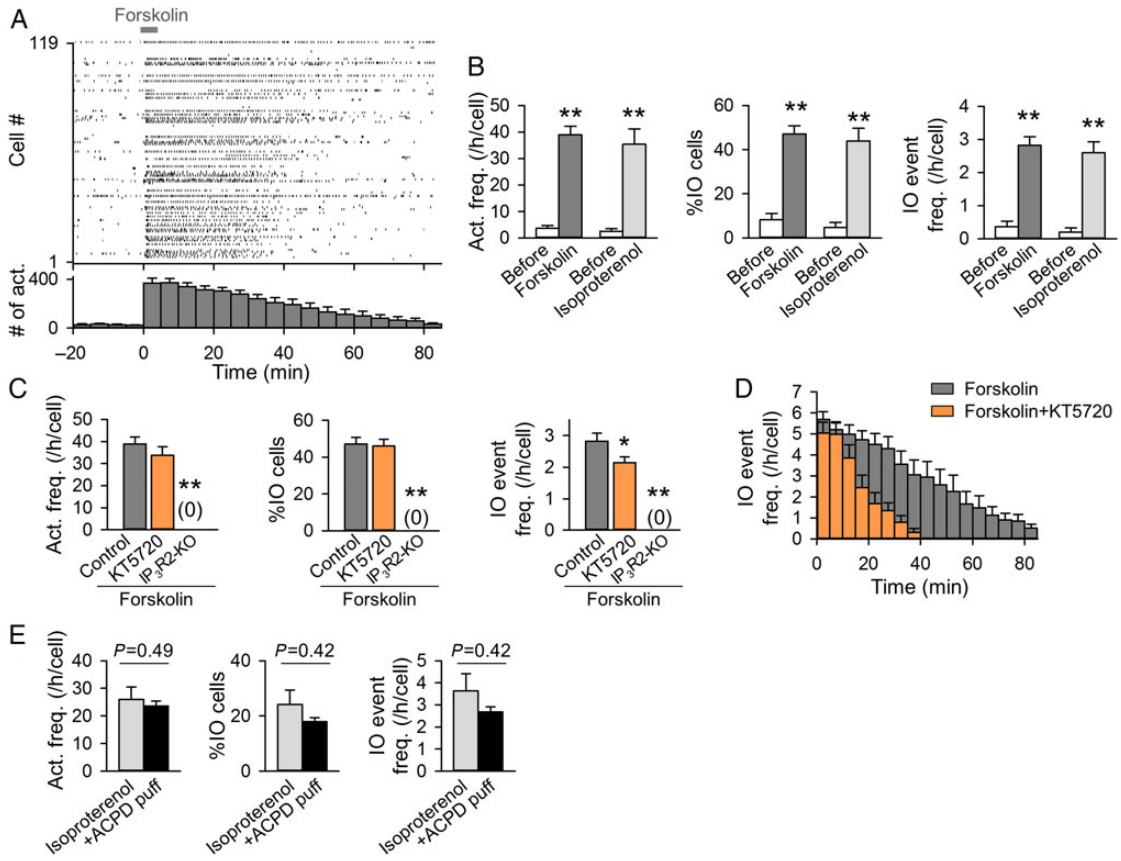

Figure 6. Activating cAMP signaling induces IOs. (*A*) Representative raster plot (*top*) and the corresponding time histogram (*bottom*) of calcium transients in response to bath application of 50 μm forskolin. Forskolin was applied at time 0–5 min. (*B*) The frequency of total transients per cell (*left*), the percentage of IO cells (*middle*), and the frequency of IO events (*right*), plotted 0–20 min before and 0–20 min after 5-min application of forskolin or 10 μm isoproterenol. $^{**}P < 0.01$ versus before, paired *t*-test. Error bars indicate the SEM of 5 slices. (*C*) The same parameters as in *B*, but for wild-type slices that were treated with forskolin alone, wild-type slices that were treated with forskolin in conjunction with KT5720 treatment, and IP3R2-KO slices that were treated with forskolin. $^{*}P < 0.05$, $^{**}P < 0.01$ versus forskolin alone, Dunnett's test after one-way ANOVA. The data were calculated over the 20-min periods before and after the 5-min application of forskolin. KT5720 was continuously bath-perfused throughout the experiments. The error bars show the SEM of 5–6 slices. (*D*) Time changes in the frequency of IO events in response to forskolin in the absence (Forskolin) and presence of KT5720 (Forskolin+KT5720). IO events were counted every 5 min. The data are presented as the mean ± SEM of 5–6 slices. (*E*) Occlusion of the effects of 10 μM isoproterenol by 100 μM ACPD. A brief ACPD puff was applied 10 min after the application of isoproterenol. The error bars show the SEM of 3 slices.

50 μm propranolol, an antagonist of β-adrenergic receptors (Supplementary Fig. 5; mean ± SEM of 5 slices; overall activity frequency: $P = 0.68$, $t_4 = 0.44$; % cells: $P = 0.37$, $t_4 = 1.00$; event frequency: $P = 0.52$, $t_4 = 0.70$, paired *t*-test). The IO-inducing effect of ACPD was occluded by preceding activation of β-adrenergic receptors by bath-applied isoproterenol (Fig. 6*E*). This result suggests that mGluR-induced and β-adrenergic receptor-induced IOs share intrinsic machinery, possibly at the level of intracellular calcium stores.

IOs as a Pathological Correlate

cAMP and calcium signals are both responsible for the regulation of cytoskeletal dynamics (Janmey 1998) and induce morphological alterations in cultured astrocytes, such as the stellation of cell bodies and the thickening of processes (Goldman and Abramson 1990; Matsuura et al. 2002). Thus, we hypothesized that IOs are associated with morphological changes in astrocytes. During calcium imaging, hippocampal slices were treated with control aCSF or aCSF containing 50 μm forskolin for 5 min, fixed with paraformaldehyde after 90 min, and immunolabeled for GFAP (Fig. 7*A*). We measured the thicknesses of GFAP-positive primary processes that extended directly from somata (Fig. 7*B*). Forskolin increased the overall thickness of the primary processes (Fig. 7*C*, *left*, spontaneous vs. forskolin: $P = 2.79 \times 10^{-5}$, $D_{427} = 0.24$, Kolmogorov–Smirnov test, $n = 153$ control and 274 forskolin-treated processes). Under naive conditions without forskolin stimulation, the primary processes of cells that exhibited IOs were significantly thicker than those of non-IO cells (Fig. 7*C*, *middle*, $P = 1.31 \times 10^{-4}$, $D_{153} = 0.35$, $n = 83$ IO and 70 non-IO processes). A similar difference was observed in forskolin-treated cells; the primary processes of cells that exhibited IOs in response to forskolin were significantly thicker than those of cells that did not (Fig. 7*C*, *right*, $P = 0.03$, $D_{274} = 0.18$, $n = 163$ IO and 111 non-IO processes). These data suggest that IOs are associated with the thickness of primary processes. We did not observe significant differences in the size of somata or in GFAP expression intensity between IO and non-IO astrocytes in forskolin-treated slices (soma size: $P = 0.42$, $D_{32} = 0.30$; GFAP intensity: $P = 0.96$, $D_{32} = 0.17$; Kolmogorov–Smirnov test; $n = 19$ IO and 13 non-IO cells).

Under pathological conditions, astrocytes become reactive and undergo morphological changes, including the thickening of processes (Sofroniew 2009; Robel et al. 2011). We examined whether astrocytes produce IOs in response to pathological stress. We treated slices with nonbubbled aCSF containing no glucose (OGD; Fig. 8*A*) and Mg^{2+}-free aCSF containing 50 μM

Downloaded from http://cercor.oxfordjournals.org/ at University of Tokyo Library on January 22, 2016

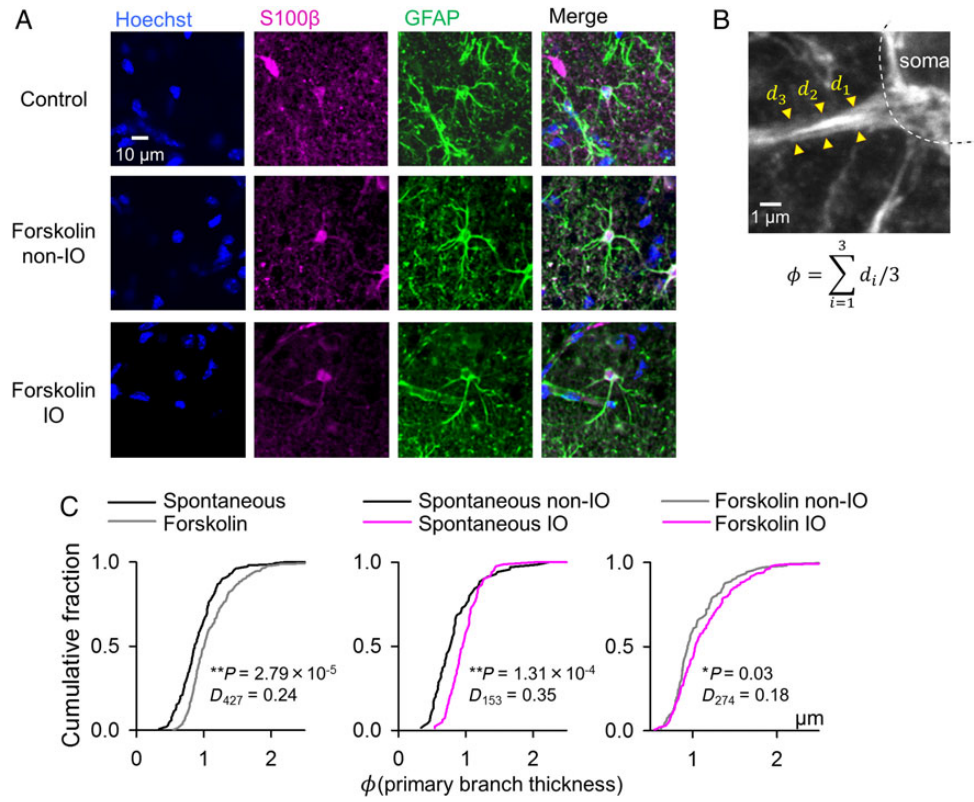

Figure 7. IOs are associated with the hypertrophy of astrocytic processes. (*A*) Immunohistochemical images for S100β and GFAP in control non-IO cells (*top*), non-IO cells (*middle*), and IO cells (*bottom*) in response to forskolin. Hoechst was used as a counterstain for nuclei. (*B*) Super-resolution confocal image illustrating the measurement of the thickness of an astrocytic process. For each branch that extended directly from the soma (primary process), the thickness was calculated by averaging the width at 3 points (d_1, d_2, and d_3) that were spaced at 1.5-μm intervals from the soma (*dashed line*). (*C*) Cumulative distributions of the thickness of primary branches in all cells, including of non-IO and IO cells in control and forskolin-treated slices (*left*), of non-IO and IO cells in control slices (*middle*), and of non-IO and IO cells in forskolin-treated slices (*right*). $^*P < 0.05$, $^{**}P < 0.01$, Kolmogorov–Smirnov test. $n = 70$ branches from 11 cells (*control non-IO*), 83 branches from 13 cells (*control IO*), 111 branches from 13 cells (*forskolin non-IO*), and 163 branches from 19 cells (*forskolin IO*).

picrotoxin, a $GABA_A$ receptor channel inhibitor (Fig. 8*B*). These 2 aCSF conditions are used as in vitro models of cerebral ischemia and epilepsy, respectively. Epileptiform hyperactive states were confirmed through calcium discharges recorded from neuropil (Fig. 8*B*, *top trace*). Both OGD and the Mg^{2+}-free aCSF increased the number of IO cells (Fig. 8*C*; OGD: $P = 0.026$, $t_6 = 2.94$; Mg^{2+}-free: $P = 0.032$, $t_4 = 3.22$) and the frequency of IO events (Fig. 8*D*; OGD: $P = 0.025$, $t_6 = 2.97$; Mg^{2+}-free: $P = 0.014$, $t_4 = 4.16$). This result was further supported by observations in an in vivo mouse carotid artery occlusion model (Supplementary Fig. 6). Astrocytes in V1 of anesthetized animals exhibited oscillatory activity as an acute response to hemispheric ischemia (% cells: 2.85% before and 57.14% after ischemia, $Z = -8.58$; Z-test for the equality of the 2 proportions). These results suggest that oscillatory activity in astrocytes is an early response to pathological conditions.

Discussion

In the present study, we analyzed the spatiotemporal patterns of astrocytic calcium activity in large-scale datasets and observed that a subset of astrocytes exhibited IOs. Because the IOs were spatiotemporally sparse, these events could not be reliably analyzed without large-scale imaging. The IOs did not require neuronal spiking activity, nor were the IO cells spatially organized or temporally synchronized among astrocytes. Therefore, IOs likely reflect single-cell dynamics that emerge independently of the states of other astrocytes. Moreover, the IOs were dependent on IP_3R-mediated intracellular calcium release and PKA-dependent signaling. The activation of cAMP alone induced prolonged oscillatory activity. Because sporadic single calcium events did not require the cAMP-PKA signaling pathway, the development of single-cycle or oscillatory calcium activity may be determined through Hopf bifurcation-like nonlinear dynamics, the critical point of which is modulated by the intracellular cAMP level (Kirk et al. 2008).

The origin of the calcium ion that is released in response to cAMP remains controversial (Grimaldi et al. 1999; Wu et al. 1999). We observed that forskolin-induced IOs were completely abolished in IP_3R2-KO mice. Therefore, at least in astrocytes, cAMP-triggered calcium elevations are mediated exclusively through intracellular calcium stores. Calcium oscillations have been documented in various cell types, including oocytes (Carroll and Swann 1992; Miyazaki et al. 1992), sperm (Fukami et al. 2003), lymphatic cells (Wilson et al. 1987), and neuronal cells, such as immature pyramidal cells and interneurons (Flint et al. 1999; Woodhall et al. 1999). Most, if not all, of these oscillations are generated through IP_3-dependent calcium release from intracellular stores. To explain how IP_3 signaling induces oscillatory patterns, several models use cAMP-calcium crosstalk (Vajanaphanich et al. 1995; Bruce et al. 2003; Siso-Nadal et al. 2009). A computational model predicted that, in the presence of cAMP, low concentrations of IP_3 could trigger calcium oscillations when they would otherwise not induce oscillations (Bugrim 1999). Consistent

Downloaded from http://cercor.oxfordjournals.org/ at University of Tokyo Library on January 22, 2016

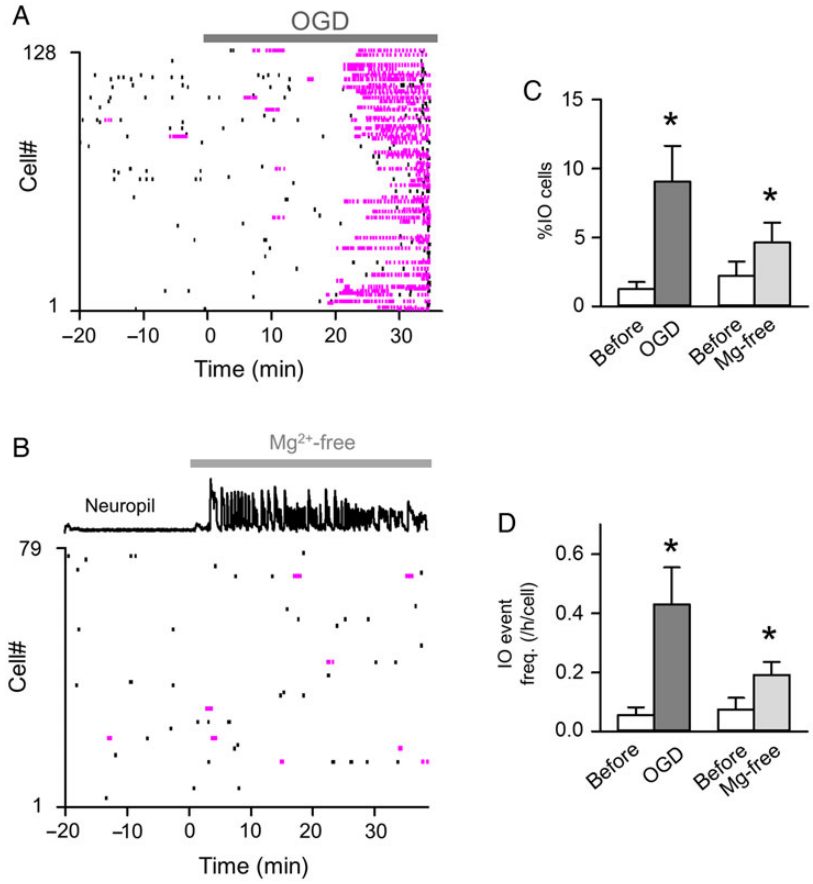

Figure 8. Increased IOs under pathological conditions. (*A*) Representative raster plot of calcium activity in response to OGD. OGD was applied from time 0 min. (*B*) Representative raster plot of calcium activity in response to Mg^{2+}-free aCSF containing 50 μM picrotoxin. Normal aCSF was changed to Mg^{2+}-free aCSF at time 0 min. The *top* trace is the mean calcium response of neuropil surrounding the recorded astrocytes, indicating that epileptiform neuronal discharges occurred under the disinhibited conditions. *Magenta dots* indicate IOs. (*C*,*D*) The percentage of IO cells (*C*) and the frequency of IO events (*D*) before and 0–15 min after the onset of OGD or Mg^{2+}-free aCSF treatment. *$P < 0.05$ versus before, paired *t*-test. Error bars show the SEM of 5–7 slices.

with this prediction, we observed that in astrocytes, IP_3R2 mediated both sporadic and IO activity, whereas the cAMP-PKA pathway was specifically involved in IOs. We could not identify the signaling molecules upstream of the cAMP pathway involved in IOs. However, astrocytes express a number of Gs-coupled receptors, such as β-adrenergic receptors (Sutin and Shao 1992), D1-like dopamine receptors (Zhang et al. 2009), and adenosine type A2a and type A2b receptors (Pilitsis and Kimelberg 1998; Chen et al. 2007). Indeed, Gs-related neuromodulators are released under pathological conditions and exert both anti- and pro-inflammatory effects (Glavin 1985; Vizi and Elenkov 2002; Burnstock 2007). These mediators could transiently or persistently increase intracellular cAMP and thereby trigger IOs in astrocytes. This idea is consistent with our finding that β-adrenergic receptor activation was sufficient to induce IOs.

PKA-dependent signaling has been reported to modulate calcium dynamics in rodent hepatocytes (Pittner and Fain 1989), blowfly salivary glands (Schmidt et al. 2008; Fechner et al. 2013), rodent parotid acinar cells (Bruce et al. 2002; Soltoff and Hedden 2010), and rabbit interstitial cells of Cajal (Drumm et al. 2014) as well as in other cell types. In these cells, PKA likely directly phosphorylates IP_3R2 channels, enhancing the sensitivity of these receptors to IP_3 (Hajnoczky et al. 1993; Wojcikiewicz and Luo 1998). In addition, intracellular calcium signaling also affects cAMP levels (Gorbunova and Spitzer 2002; Willoughby and Cooper 2006). This positive feed-forward loop between the cAMP-PKA and IP_3R2-calcium pathways might contribute to the generation and elongation of IOs.

Despite a large body of literature regarding cAMP-calcium interactions in other cell types, a limited number of studies have focused on cAMP in astrocytes; these studies have demonstrated the involvement of cAMP-calcium crosstalk in glycogenolysis and in the production of inflammatory molecules in cultured astrocytes (Hsiao et al. 2007; Juric et al. 2008; Muller et al. 2014). Using acute slices, we observed cAMP-dependent IOs in astrocytes and implicated these events as responses to pathological stress. These results are consistent with previous studies that have suggested that reactive astrogliosis requires intracellular calcium (Gao et al. 2013; Kanemaru et al. 2013) and cAMP signaling (Kaneko et al. 1994; Segovia et al. 1994; Schubert et al. 2000). The calcium activity level is known to increase in several animal models of neuronal diseases (Ding et al. 2007; Takano et al. 2007; Kuchibhotla et al. 2009); however, little is known about the temporal patterns of calcium dynamics. Our work suggests that the oscillatory patterns are associated with pathological stress.

Recent evidence has demonstrated that astrocytes release and respond to glutamate in a specific manner (Woo et al. 2012; Sun et al. 2013). Indeed, we observed that IOs were attenuated by a metabotropic glutamate receptor antagonist but not by TTX. We hypothesize that ambient extracellular glutamate that is released either from astrocytes themselves or by neurons in an action potential-independent manner triggers IOs. Furthermore, it is

Downloaded from http://cercor.oxfordjournals.org/ at University of Tokyo Library on January 22, 2016

possible that the enhancement of IOs under pathological states influences neuronal function. Because astrocytes release various transmitters in response to pathological stimuli, IOs could modulate the activity of adjacent neurons, thereby alleviating or aggravating the pathological malfunction of neurons. This idea could be tested after the development of a new technique that can specifically manipulate the temporal dynamics of calcium responses in astrocytes. It also remains to be clarified whether morphological changes in astrocytes actively regulate astrocytic function in pathological states. Given that astrocytes are rapidly activated during the early stages of pathology, it is possible that the morphological changes may enhance or even trigger the transformation of astrocytes from a quiescent to an active state. Thus, if the reactivation of astrocytes enhances oscillatory patterns, a strong feedforward loop of astrocytic reactivation may be formed. This notion could also be addressed using a technique that manipulates astrocytic calcium dynamics

Because of the technical limitations of large-scale imaging using a low-magnification objective, we observed calcium transients primarily in the somata of the astrocytes. At higher magnification, however, we also identified IOs as a complex intercellular interaction between somata and peripheral processes. Local oscillations also existed in primary processes. These data, although preliminary, suggest that oscillations are coordinated with wave-like intercellular propagations of calcium transients that involve astrocytes at the whole-cell level. Although astrocytic calcium activity is sensitive to developmental changes in receptor expression (Sun et al. 2013), our experiments primarily employed slice preparations obtained from juvenile animals. However, in some of the experiments, we also observed that IOs occurred in awake and anesthetized adult animals. Therefore, IOs likely represent a common, fundamental pattern of astrocytic activity that occurs independently of developmental stage or experimental preparation.

Supplementary Material

Supplementary material can be found at: http://www.cercor.oxfordjournals.org/.

Funding

This work was supported through grants from Kaken-hi (22115003; 2625000), Takeda Science Foundation, and Kobayashi International Scholarship Foundation.

Notes

Conflict of Interest: None declared.

References

Aguado F, Espinosa-Parrilla JF, Carmona MA, Soriano E. 2002. Neuronal activity regulates correlated network properties of spontaneous calcium transients in astrocytes in situ. J Neurosci. 22:9430–9444.

Agulhon C, Sun MY, Murphy T, Myers T, Lauderdale K, Fiacco TA. 2012. Calcium signaling and gliotransmission in normal vs. reactive astrocytes. Front Pharmacol. 3:139.

Bruce JI, Shuttleworth TJ, Giovannucci DR, Yule DI. 2002. Phosphorylation of inositol 1,4,5-trisphosphate receptors in parotid acinar cells. A mechanism for the synergistic effects of cAMP on Ca^{2+} signaling. J Biol Chem. 277:1340–1348.

Bruce JI, Straub SV, Yule DI. 2003. Crosstalk between cAMP and Ca^{2+} signaling in non-excitable cells. Cell Calcium. 34:431–444.

Bugrim AE. 1999. Regulation of Ca^{2+} release by cAMP-dependent protein kinase. A mechanism for agonist-specific calcium signaling? Cell Calcium. 25:219–226.

Burnstock G. 2007. Physiology and pathophysiology of purinergic neurotransmission. Physiol Rev. 87:659–797.

Carroll J, Swann K. 1992. Spontaneous cytosolic calcium oscillations driven by inositol trisphosphate occur during in vitro maturation of mouse oocytes. J Biol Chem. 267:11196–11201.

Chatton JY, Cao Y, Liu H, Stucki JW. 1998. Permissive role of cAMP in the oscillatory Ca^{2+} response to inositol 1,4,5-trisphosphate in rat hepatocytes. Biochem J. 330:1411–1416.

Chen JF, Sonsalla PK, Pedata F, Melani A, Domenici MR, Popoli P, Geiger J, Lopes LV, de Mendonca A. 2007. Adenosine A2A receptors and brain injury: broad spectrum of neuroprotection, multifaceted actions and "fine tuning" modulation. Prog Neurobiol. 83:310–331.

Ding S, Fellin T, Zhu Y, Lee SY, Auberson YP, Meaney DF, Coulter DA, Carmignoto G, Haydon PG. 2007. Enhanced astrocytic Ca^{2+} signals contribute to neuronal excitotoxicity after status epilepticus. J Neurosci. 27:10674–10684.

Drumm BT, Sergeant GP, Hollywood MA, Thornbury KD, McHale NG, Harvey BJ. 2014. The role of cAMP dependent protein kinase in modulating spontaneous intracellular Ca^{2+} waves in interstitial cells of Cajal from the rabbit urethra. Cell Calcium. 56:181–187.

Fechner L, Baumann O, Walz B. 2013. Activation of the cyclic AMP pathway promotes serotonin-induced Ca^{2+} oscillations in salivary glands of the blowfly Calliphora vicina. Cell Calcium. 53:94–101.

Fiacco TA, Agulhon C, McCarthy KD. 2009. Sorting out astrocyte physiology from pharmacology. Annu Rev Pharmacol Toxicol. 49:151–174.

Flint AC, Dammerman RS, Kriegstein AR. 1999. Endogenous activation of metabotropic glutamate receptors in neocortical development causes neuronal calcium oscillations. Proc Natl Acad Sci USA. 96:12144–12149.

Fukami K, Yoshida M, Inoue T, Kurokawa M, Fissore RA, Yoshida N, Mikoshiba K, Takenawa T. 2003. Phospholipase Cdelta4 is required for Ca^{2+} mobilization essential for acrosome reaction in sperm. J Cell Biol. 161:79–88.

Funayama K, Minamisawa G, Matsumoto N, Ban H, Chan AW, Matsuki N, Murphy TH, Ikegaya Y. 2015. Neocortical rebound depolarization enhances visual perception. PLoS Biol. 13:e1002231.

Gao K, Wang CR, Jiang F, Wong AY, Su N, Jiang JH, Chai RC, Vatcher G, Teng J, Chen J, et al. 2013. Traumatic scratch injury in astrocytes triggers calcium influx to activate the JNK/c-Jun/AP-1 pathway and switch on GFAP expression. Glia. 61:2063–2077.

Giaume C, Koulakoff A, Roux L, Holcman D, Rouach N. 2010. Astroglial networks: a step further in neuroglial and gliovascular interactions. Nat Rev Neurosci. 11:87–99.

Giaume C, Liu X. 2012. From a glial syncytium to a more restricted and specific glial networking. J Physiol Paris. 106:34–39.

Girouard H, Bonev AD, Hannah RM, Meredith A, Aldrich RW, Nelson MT. 2010. Astrocytic endfoot Ca^{2+} and BK channels determine both arteriolar dilation and constriction. Proc Natl Acad Sci USA. 107:3811–3816.

Glavin GB. 1985. Stress and brain noradrenaline: a review. Neurosci Biobehav Rev. 9:233–243.

Goldman JE, Abramson B. 1990. Cyclic AMP-induced shape changes of astrocytes are accompanied by rapid depolymerization of actin. Brain Res. 528:189–196.

Gorbunova YV, Spitzer NC. 2002. Dynamic interactions of cyclic AMP transients and spontaneous Ca^{2+} spikes. Nature. 418:93–96.

Downloaded from http://cercor.oxfordjournals.org/ at University of Tokyo Library on January 22, 2016

Gordon GR, Choi HB, Rungta RL, Ellis-Davies GC, MacVicar BA. 2008. Brain metabolism dictates the polarity of astrocyte control over arterioles. Nature. 456:745–749.

Grimaldi M, Favit A, Alkon DL. 1999. cAMP-induced cytoskeleton rearrangement increases calcium transients through the enhancement of capacitative calcium entry. J Biol Chem. 274:33557–33564.

Hajnoczky G, Gao E, Nomura T, Hoek JB, Thomas AP. 1993. Multiple mechanisms by which protein kinase A potentiates inositol 1,4,5-trisphosphate-induced Ca^{2+} mobilization in permeabilized hepatocytes. Biochem J. 293(Pt 2):413–422.

Hamilton NB, Attwell D. 2010. Do astrocytes really exocytose neurotransmitters? Nat Rev Neurosci. 11:227–238.

Henneberger C, Papouin T, Oliet SH, Rusakov DA. 2010. Long-term potentiation depends on release of D-serine from astrocytes. Nature. 463:232–236.

Hirase H, Qian L, Bartho P, Buzsaki G. 2004. Calcium dynamics of cortical astrocytic networks in vivo. PLoS Biol. 2:E96.

Holtzclaw LA, Pandhit S, Bare DJ, Mignery GA, Russell JT. 2002. Astrocytes in adult rat brain express type 2 inositol 1,4,5-trisphosphate receptors. Glia. 39:69–84.

Hsiao HY, Mak OT, Yang CS, Liu YP, Fang KM, Tzeng SF. 2007. TNF-alpha/IFN-gamma-induced iNOS expression increased by prostaglandin E2 in rat primary astrocytes via EP2-evoked cAMP/PKA and intracellular calcium signaling. Glia. 55:214–223.

Ikegaya Y, Aaron G, Cossart R, Aronov D, Lampl I, Ferster D, Yuste R. 2004. Synfire chains and cortical songs: temporal modules of cortical activity. Science. 304:559–564.

Ikegaya Y, Le Bon-Jego M, Yuste R. 2005. Large-scale imaging of cortical network activity with calcium indicators. Neurosci Res. 52:132–138.

Ishikawa D, Matsumoto N, Sakaguchi T, Matsuki N, Ikegaya Y. 2014. Operant conditioning of synaptic and spiking activity patterns in single hippocampal neurons. J Neurosci. 34:5044–5053.

Janmey PA. 1998. The cytoskeleton and cell signaling: component localization and mechanical coupling. Physiol Rev. 78:763–781.

Jourdain P, Bergersen LH, Bhaukaurally K, Bezzi P, Santello M, Domercq M, Matute C, Tonello F, Gundersen V, Volterra A. 2007. Glutamate exocytosis from astrocytes controls synaptic strength. Nat Neurosci. 10:331–339.

Juric DM, Loncar D, Carman-Krzan M. 2008. Noradrenergic stimulation of BDNF synthesis in astrocytes: mediation via alpha1- and beta1/beta2-adrenergic receptors. Neurochem Int. 52:297–306.

Kaneko R, Hagiwara N, Leader K, Sueoka N. 1994. Glial-specific cAMP response of the glial fibrillary acidic protein gene cell lines. Proc Natl Acad Sci USA. 91:4529–4533.

Kanemaru K, Kubota J, Sekiya H, Hirose K, Okubo Y, Iino M. 2013. Calcium-dependent N-cadherin up-regulation mediates reactive astrogliosis and neuroprotection after brain injury. Proc Natl Acad Sci USA. 110:11612–11617.

Kase H, Iwahashi K, Nakanishi S, Matsuda Y, Yamada K, Takahashi M, Murakata C, Sato A, Kaneko M. 1987. K-252 compounds, novel and potent inhibitors of protein kinase C and cyclic nucleotide-dependent protein kinases. Biochem Biophys Res Commun. 142:436–440.

Kawamata H, Ng SK, Diaz N, Burstein S, Morel L, Osgood A, Sider B, Higashimori H, Haydon PG, Manfredi G, et al. 2014. Abnormal intracellular calcium signaling and SNARE-dependent exocytosis contributes to SOD1G93A astrocyte-mediated toxicity in amyotrophic lateral sclerosis. J Neurosci. 34:2331–2348.

Kirk PD, Toni T, Stumpf MP. 2008. Parameter inference for biochemical systems that undergo a Hopf bifurcation. Biophys J. 95:540–549.

Kuchibhotla KV, Lattarulo CR, Hyman BT, Bacskai BJ. 2009. Synchronous hyperactivity and intercellular calcium waves in astrocytes in Alzheimer mice. Science. 323:1211–1215.

Kuga N, Sasaki T, Takahara Y, Matsuki N, Ikegaya Y. 2011. Large-scale calcium waves traveling through astrocytic networks *in vivo*. J Neurosci. 31:2607–2614.

Lee W, Reyes RC, Gottipati MK, Lewis K, Lesort M, Parpura V, Gray M. 2013. Enhanced Ca^{2+}-dependent glutamate release from astrocytes of the BACHD Huntington's disease mouse model. Neurobiol Dis. 58:192–199.

Li YX, Keizer J, Stojilkovic SS, Rinzel J. 1995. Ca^{2+} excitability of the ER membrane: an explanation for IP3-induced Ca^{2+} oscillations. Am J Physiol. 269:C1079–C1092.

Matsuura S, Ikegaya Y, Yamada MK, Nishiyama N, Matsuki N. 2002. Endothelin downregulates the glutamate transporter GLAST in cAMP-differentiated astrocytes in vitro. Glia. 37:178–182.

Mikoshiba K. 2011. Role of IP(3) receptor in development. Cell Calcium. 49:331–340.

Min R, Nevian T. 2012. Astrocyte signaling controls spike timing-dependent depression at neocortical synapses. Nat Neurosci. 15:746–753.

Miyazaki S, Yuzaki M, Nakada K, Shirakawa H, Nakanishi S, Nakade S, Mikoshiba K. 1992. Block of Ca^{2+} wave and Ca^{2+} oscillation by antibody to the inositol 1,4,5-trisphosphate receptor in fertilized hamster eggs. Science. 257:251–255.

Muller MS, Fox R, Schousboe A, Waagepetersen HS, Bak LK. 2014. Astrocyte glycogenolysis is triggered by store-operated calcium entry and provides metabolic energy for cellular calcium homeostasis. Glia. 62:526–534.

Mulligan SJ, MacVicar BA. 2004. Calcium transients in astrocyte endfeet cause cerebrovascular constrictions. Nature. 431:195–199.

Navarrete M, Araque A. 2010. Endocannabinoids potentiate synaptic transmission through stimulation of astrocytes. Neuron. 68:113–126.

Nett WJ, Oloff SH, McCarthy KD. 2002. Hippocampal astrocytes in situ exhibit calcium oscillations that occur independent of neuronal activity. J Neurophysiol. 87:528–537.

Orr AG, Hsiao EC, Wang MM, Ho K, Kim DH, Wang X, Guo W, Kang J, Yu GQ, Adame A, et al. 2015. Astrocytic adenosine receptor A2A and Gs-coupled signaling regulate memory. Nat Neurosci. 18:423–434.

Parri HR, Gould TM, Crunelli V. 2001. Spontaneous astrocytic Ca^{2+} oscillations in situ drive NMDAR-mediated neuronal excitation. Nat Neurosci. 4:803–812.

Pilitsis JG, Kimelberg HK. 1998. Adenosine receptor mediated stimulation of intracellular calcium in acutely isolated astrocytes. Brain Res. 798:294–303.

Pittner RA, Fain JN. 1989. Exposure of cultured hepatocytes to cyclic AMP enhances the vasopressin-mediated stimulation of inositol phosphate production. Biochem J. 257:455–460.

Reeves AM, Shigetomi E, Khakh BS. 2011. Bulk loading of calcium indicator dyes to study astrocyte physiology: key limitations and improvements using morphological maps. J Neurosci. 31:9353–9358.

Robel S, Berninger B, Gotz M. 2011. The stem cell potential of glia: lessons from reactive gliosis. Nat Rev Neurosci. 12:88–104.

Salm AK, McCarthy KD. 1992. The evidence for astrocytes as a target for central noradrenergic activity: expression of adrenergic receptors. Brain Res Bull. 29:265–275.

Sasaki T, Kuga N, Namiki S, Matsuki N, Ikegaya Y. 2011. Locally synchronized astrocytes. Cereb Cortex. 21:1889–1900.

Sasaki T, Matsuki N, Ikegaya Y. 2011. Action-potential modulation during axonal conduction. Science. 331:599–601.

Downloaded from http://cercor.oxfordjournals.org/ at University of Tokyo Library on January 22, 2016

Sasaki T, Matsuki N, Ikegaya Y. 2007. Metastability of active CA3 networks. J Neurosci. 27:517–528.

Sasaki T, Takahashi N, Matsuki N, Ikegaya Y. 2008. Fast and accurate detection of action potentials from somatic calcium fluctuations. J Neurophysiol. 100:1668–1676.

Schmidt R, Baumann O, Walz B. 2008. cAMP potentiates InsP3-induced Ca^{2+} release from the endoplasmic reticulum in blowfly salivary glands. BMC Physiol. 8:10.

Schubert P, Morino T, Miyazaki H, Ogata T, Nakamura Y, Marchini C, Ferroni S. 2000. Cascading glia reactions: a common pathomechanism and its differentiated control by cyclic nucleotide signaling. Ann N Y Acad Sci. 903:24–33.

Segovia J, Lawless GM, Tillakaratne NJ, Brenner M, Tobin AJ. 1994. Cyclic AMP decreases the expression of a neuronal marker (GAD67) and increases the expression of an astroglial marker (GFAP) in C6 cells. J Neurochem. 63:1218–1225.

Sharp AH, Nucifora FC Jr, Blondel O, Sheppard CA, Zhang C, Snyder SH, Russell JT, Ryugo DK, Ross CA. 1999. Differential cellular expression of isoforms of inositol 1,4,5-triphosphate receptors in neurons and glia in brain. J Comp Neurol. 406:207–220.

Siso-Nadal F, Fox JJ, Laporte SA, Hebert TE, Swain PS. 2009. Cross-talk between signaling pathways can generate robust oscillations in calcium and cAMP. PLoS One. 4:e7189.

Sofroniew MV. 2009. Molecular dissection of reactive astrogliosis and glial scar formation. Trends Neurosci. 32:638–647.

Soltoff SP, Hedden L. 2010. Isoproterenol and cAMP block ERK phosphorylation and enhance $[Ca^{2+}]_i$ increases and oxygen consumption by muscarinic receptor stimulation in rat parotid and submandibular acinar cells. J Biol Chem. 285:13337–13348.

Sun W, McConnell E, Pare JF, Xu Q, Chen M, Peng W, Lovatt D, Han X, Smith Y, Nedergaard M. 2013. Glutamate-dependent neuroglial calcium signaling differs between young and adult brain. Science. 339:197–200.

Sutin J, Shao Y. 1992. Resting and reactive astrocytes express adrenergic receptors in the adult rat brain. Brain Res Bull. 29:277–284.

Takano T, Han X, Deane R, Zlokovic B, Nedergaard M. 2007. Two-photon imaging of astrocytic Ca^{2+} signaling and the microvasculature in experimental mice models of Alzheimer's disease. Ann N Y Acad Sci. 1097:40–50.

Takata N, Mishima T, Hisatsune C, Nagai T, Ebisui E, Mikoshiba K, Hirase H. 2011. Astrocyte calcium signaling transforms cholinergic modulation to cortical plasticity in vivo. J Neurosci. 31:18155–18165.

Thomas D, Tovey SC, Collins TJ, Bootman MD, Berridge MJ, Lipp P. 2000. A comparison of fluorescent Ca^{2+} indicator properties and their use in measuring elementary and global Ca^{2+} signals. Cell Calcium. 28:213–223.

Tymianski M, Bernstein GM, Abdel-Hamid KM, Sattler R, Velumian A, Carlen PL, Razavi H, Jones OT. 1997. A novel use for a carbodiimide compound for the fixation of fluorescent and non-fluorescent calcium indicators in situ following physiological experiments. Cell Calcium. 21:175–183.

Vajanaphanich M, Schultz C, Tsien RY, Traynor-Kaplan AE, Pandol SJ, Barrett KE. 1995. Cross-talk between calcium and cAMP-dependent intracellular signaling pathways. Implications for synergistic secretion in T84 colonic epithelial cells and rat pancreatic acinar cells. J Clinical Invest. 96:386–393.

Vardjan N, Kreft M, Zorec R. 2014. Dynamics of beta-adrenergic/cAMP signaling and morphological changes in cultured astrocytes. Glia. 62:566–579.

Vizi ES, Elenkov IJ. 2002. Nonsynaptic noradrenaline release in neuro-immune responses. Acta Biologica Hungarica. 53:229–244.

Volterra A, Liaudet N, Savtchouk I. 2014. Astrocyte Ca^{2+} signalling: an unexpected complexity. Nat Rev Neurosci. 15:327–335.

Willoughby D, Cooper DM. 2006. Ca^{2+} stimulation of adenylyl cyclase generates dynamic oscillations in cyclic AMP. J Cell Sci. 119:828–836.

Wilson HA, Greenblatt D, Poenie M, Finkelman FD, Tsien RY. 1987. Crosslinkage of B lymphocyte surface immunoglobulin by anti-Ig or antigen induces prolonged oscillation of intracellular ionized calcium. J Exp Med. 166:601–606.

Wojcikiewicz RJ, Furuichi T, Nakade S, Mikoshiba K, Nahorski SR. 1994. Muscarinic receptor activation down-regulates the type I inositol 1,4,5-trisphosphate receptor by accelerating its degradation. J Biol Chem. 269:7963–7969.

Wojcikiewicz RJ, Luo SG. 1998. Phosphorylation of inositol 1,4,5-trisphosphate receptors by cAMP-dependent protein kinase. Type I, II, and III receptors are differentially susceptible to phosphorylation and are phosphorylated in intact cells. J Biol Chem. 273:5670–5677.

Woo DH, Han KS, Shim JW, Yoon BE, Kim E, Bae JY, Oh SJ, Hwang EM, Marmorstein AD, Bae YC, et al. 2012. TREK-1 and Best1 channels mediate fast and slow glutamate release in astrocytes upon GPCR activation. Cell. 151:25–40.

Woodhall G, Gee CE, Robitaille R, Lacaille JC. 1999. Membrane potential and intracellular Ca^{2+} oscillations activated by mGluRs in hippocampal stratum oriens/alveus interneurons. J Neurophysiol. 81:371–382.

Woods NM, Cuthbertson KS, Cobbold PH. 1986. Repetitive transient rises in cytoplasmic free calcium in hormone-stimulated hepatocytes. Nature. 319:600–602.

Wu ML, Chen WH, Liu IH, Tseng CD, Wang SM. 1999. A novel effect of cyclic AMP on capacitative Ca^{2+} entry in cultured rat cerebellar astrocytes. J Neurochem. 73:1318–1328.

Zhang X, Zhou Z, Wang D, Li A, Yin Y, Gu X, Ding F, Zhen X, Zhou J. 2009. Activation of phosphatidylinositol-linked D1-like receptor modulates FGF-2 expression in astrocytes via IP3-dependent Ca^{2+} signaling. J Neurosci. 29:7766–7775.

Downloaded from http://cercor.oxfordjournals.org/ at University of Tokyo Library on January 22, 2016